Supporting Information

Dynamics of Glycine Dications in The Gas Phase: Ultrafast Intramolecular Hydrogen Migration *vs.* Coulomb Repulsion

Sylvain Maclot, Dariusz Grzegorz Piekarski, Alicja Domaracka, Alain Méry, Violaine Vizcaino, Lamri Adoui, Fernando Martín, Manuel Alcamí, Bernd A. Huber, Patrick Rousseau and Sergio Díaz-Tendero

October 21, 2013

S.I.1 Experimental details

The experimental details are described in detail elsewhere,[1] thus only a short description is given here. Experiments were performed with a crossed beams device,[2] where a pulsed beam of highly charged Xe^{25+} ions interacts with a beam of neutral glycine molecules produced by evaporation of commercial high purity powder of glycine and glycine-2-2-d_2 in an oven kept at 400K. After the interaction, the cationic products are orthogonally extracted into a linear time-of-flight mass spectrometer. Time-of-flight spectra are recorded in an event-by-event mode allowing to measure the correlation between the charged fragments proceeding from a single ion-molecule collision.[1] Table 1 shows the relative intensities with the corresponding assignation of the correlation islands in the regions of interest in the coincidence map shown in Figure 2 in the main article. Figure 1 shows the mass spectrum of the cationic products obtained by fragmentation of the glycine dication in two charged fragments after the interaction of neutral glycine with Xe^{25+} ions at the energy of 387.5 keV.

S.I.2 Theoretical methods

Quantum chemistry calculations were carried out using the density functional theory (DFT). In particular, geometry optimizations were performed using the B3LYP functional, which combines the Becke's three parameter nonlocal hybrid exchange potential[3] with the nonlocal correlation functional of Lee, Yang and Parr.[4] This functional has been used in combination with the 6-311++G(d,p) basis set. This level of theory has been shown to give accurate results for similar systems.[5] Harmonic vibrational frequencies have been also evaluated at the same level to characterize minima and transition states in the potential energy surface (PES) and to compute the Zero Point Energy (ZPE) correction. For the obtained transition states, intrinsic reaction coordinate (IRC) calculations have been also carried out to verify the minima they connect. Figure 4 in the main article shows the most important points in the PES that explain the fragmentation paths of doubly-ionized glycine. Figures 2, 3 and 4 here, show complementary information obtained on the exploration of the potential energy surface.

Ab initio molecular dynamics (AIMD) calculations were performed using the Atom-centered Density Matrix Propagation method (ADMP),[6–8] at the B3LYP/6-31++G(d,p) level of theory. To ensure the adiabaticiy during the propagation we chose a time step of $\Delta t = 0.1$ fs and fictitious electron mass of 0.1 amu. We take the geometry of the five most stable conformers of neutral glycine and from them we run simulations increasing the internal vibrational energy (0.001, 0.005, 0.01, 0.02, 0.03, 0.04, 0.05, 0.06, 0.07, 0.08, 0.09, 0.1, 0.11, 0.12, 0.13, 0.14 and 0.15 hartrees). The initial velocity of the atoms were randomly selected for each trajectory, isomer and value of the internal energy. A total of 1700 trajectories were performed (20 trajectories for each of the 5 isomers considering 17 values of internal excitation energy). We extract statistics from them by analyzing the fragments produced in the simulations at a propagation time of $t_{\max}$ =200 fs. In particular we have observed eight possible exit channels in our simulations:

(a) $Gly^{2+} \rightarrow NH_2CH_2^+ + COOH^+$

(b) $Gly^{2+} \rightarrow NH_3CH^+ + COOH^+$

(c) $Gly^{2+} \rightarrow [NH_2 - CH - C(OH)_2]^{2+}$

(d) $Gly^{2+} \rightarrow [NH_3 - CH - COOH]^{2+}$

(e) $Gly^{2+} \rightarrow NH_2CHCOOH^+ + H^+$

(f) $Gly^{2+} \rightarrow NH_3CHOH^{2+} + CO$

(g) $Gly^{2+} \rightarrow NH_2CHCO^+ + H_2O^+$ / $NH_2CHCO^{2+} + H_2O$

(h) $Gly^{2+} \rightarrow NH_2C^+ + H_2 + COOH^+$

Processes (a) and (b) are Coulomb explosion, (c) and (d) are isomerization, (e) is H^+ loss, (f) is CO loss, (g) is H_2O or H_2O^+ loss and (h) is a Coulomb explosion combined with a H_2 loss, exit channels. The results of the statistics are shown in Table 2. As a general conclusion, Coulomb explosion (a-b) is observed in 97.94%, isomerization (c-d) in 1,65% and the rest of the processes (e-h) in 0.41% of the total number of simulations performed.

All the calculations were performed using the Gaussian09 program.[9]

References

[1] Capron, M. et al. *Chem. Eur. J.* **2012**, *18*, 9321–9332.

[2] Bergen, T.; Biquard, X.; Brenac, A.; Chandezon, F.; Huber, B. A.; Jalabert, D.; Lebius, H.; Maurel, M.; Monnand, E.; Opitz, J.; Pesnelle, A.; Pras, B.; Ristori, C.; Rocco, J. C. *Rev. Sci. Instrum.* **1999**, *70*, 3244–3253.

[3] Becke, A. D. *J. Chem. Phys.* **1993**, *98*, 5648–5652.

[4] Lee, C.; Yang, W.; Parr, R. G. *Phys. Rev. B* **1988**, *37*, 785–789.

[5] Gil, A.; Simon, S.; Rodríguez-Santiago, L.; Bertrán, J.; Sodupe, M. *J. Chem. Theory Comput.* **2007**, *3*, 2210–2220.

[6] Schlegel, H. B.; Millam, J. M.; Iyengar, S. S.; Voth, G. A.; Daniels, A. D.; Scuseria, G. E.; Frisch, M. J. *J. Chem. Phys.* **2001**, *114*, 9758–9763.

[7] Iyengar, S. S.; Schlegel, H. B.; Millam, J. M.; Voth, G. A.; Scuseria, G. E.; Frisch, M. J. *J. Chem. Phys.* **2001**, *115*, 10291–10302.

[8] Schlegel, H. B.; Iyengar, S. S.; Li, X.; Millam, J. M.; Voth, G. A.; Scuseria, G. E.; Frisch, M. J. *J. Chem. Phys.* **2002**, *117*, 8694–8704.

[9] Frisch, M. J. et al. Gaussian 09 Revision B.01. 2010; Gaussian Inc. Wallingford CT 2009.

S.I.3 Results

M1	M2	Relative Intensity	Assignation
18	55	0.05%	H_2O^+/NH_2CHCO^+
18	57	0.14%	$H_2O^+/HNCCO^+$
27	28	1.04%	HNC^+/CO^+
27	29	0.93%	HNC^+/COH^+
27	30	0.36%	HNC^+/COH_2^+
27	45	0.91%	$HNC^+/COOH^+$
28	29	5.20%	$NHCH^+/COH^+$ NH_2CH^+/CO^+
28	30	4.77%	$CO^+/NH_2CH_2^+$ $NHCH^+/COH_2^+$
28	45	7.71%	$NHCH^+/COOH^+$
29	30	2.05%	$COH^+/NH_2CH_2^+$ NH_2CH^+/COH_2^+
29	45	2.37%	$NH_2CH^+/COOH^+$
30	45	3.82%	$NH_2CH_2^+/COOH^+$

Table 1: Assignation of the correlation islands corresponding to the regions of interest in the coincidence map (see Fig. 2 in the main article). Relative intensities are given in percentage of the total intensity of the map.

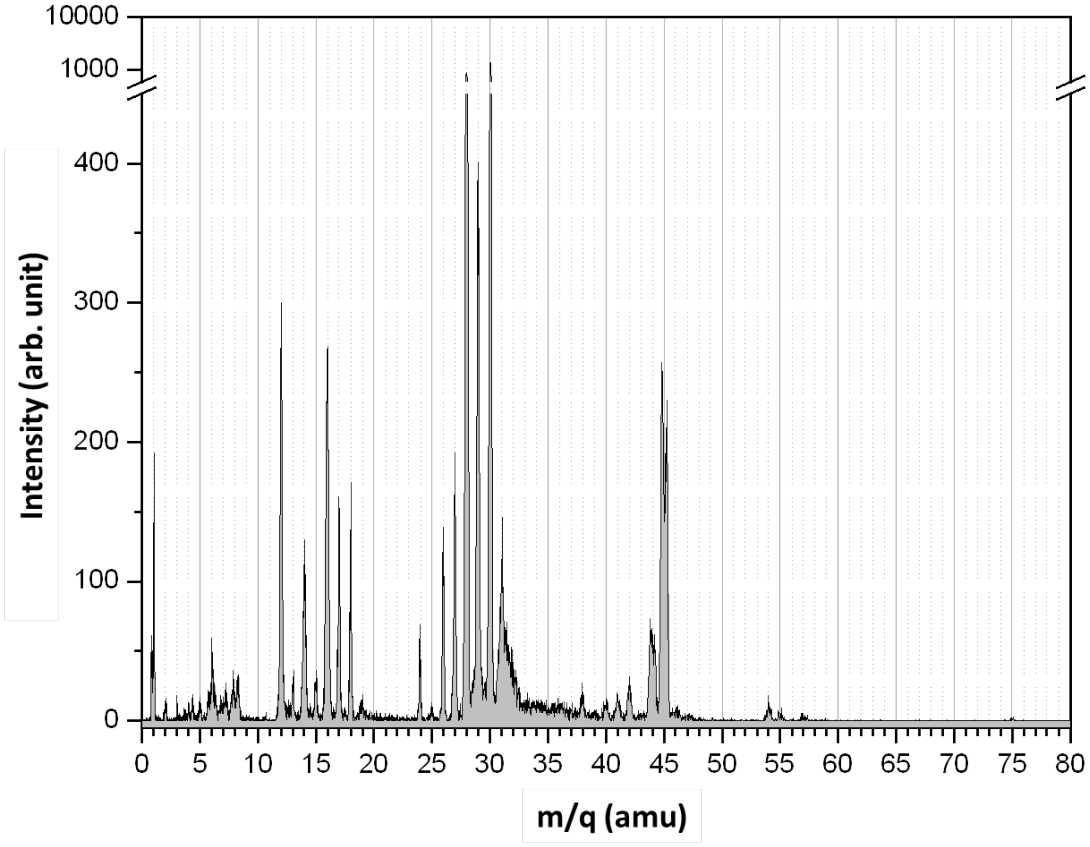

Figure 1: Mass spectrum of the cationic products obtained by fragmentation of the glycine dication in two charged fragments after the interaction of neutral glycine with Xe^{25+} ions at the energy of 387.5 keV.

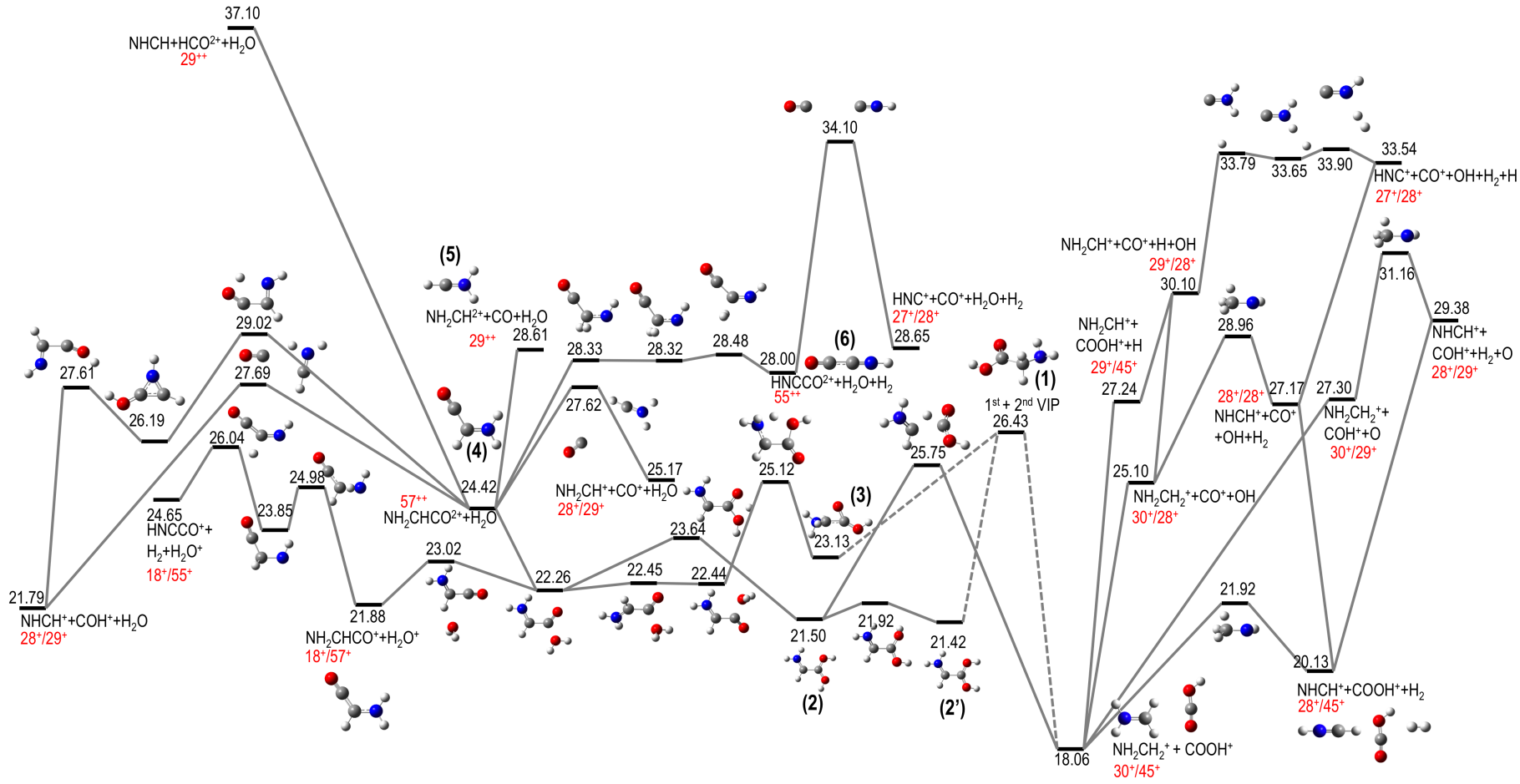

Figure 2: Most relevant fragmentation pathways for doubly positively charged glycine. Relative energies, ΔE, are given in eV at the DFT-B3LYP/6-311++G(d,p) level of theory including the zero point energy correction with respect to the most stable isomer of the neutral molecule. Key structures as cited in the article are labelled as (1), (2), etc. Coincidence notation is also included, e.g. $30^+/45^+$.
Left part: fragmentation channels leading to doubly charged species after H migration and neutral moieties lost.
Right part: framentation channels leading to coincident measurements after Coulomb explosion.
Other channels are shown in Fig. 3, isomerization of doubly charged glycine, and in Fig. 4, Coulomb explosion after H migration.

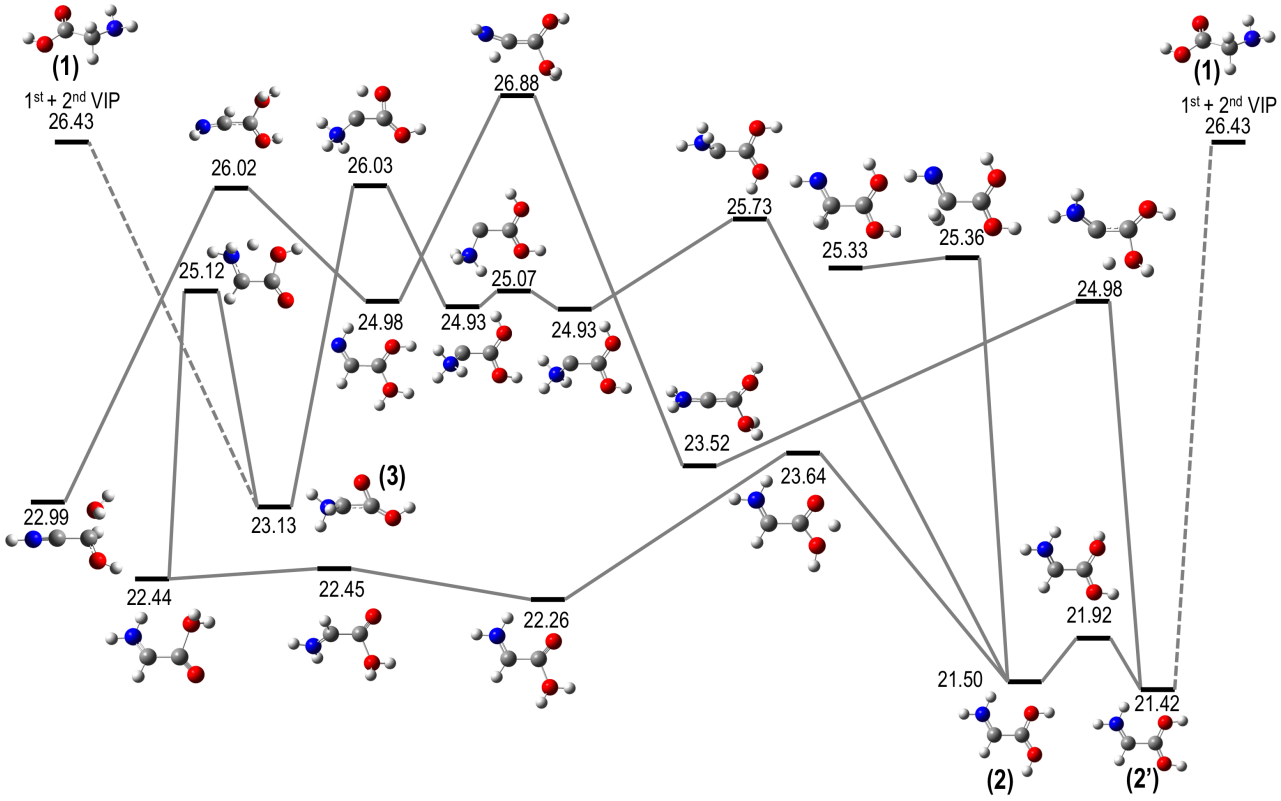

Figure 3: Isomerization pathways for doubly positively charged glycine. Relative energies, ΔE, are given in eV at the DFT-B3LYP/6-311++G(d,p) level of theory including the zero point energy correction with respect to the most stable isomer of the neutral molecule. Key structures as cited in the article are labelled as (1), (2), etc. Notice that the atomic arangement of the inital glycine molecule, NH_2CH_2COOH does not exist as stable isomer in dicationic glycine: geminal diol $-C(OH)_2$ (obtained from (1) in the right part of the figure) in and/or $-NH_3$ terminations (obtained from (1) in the left part of the figure) stabilize the charge$-$charge repulsion.

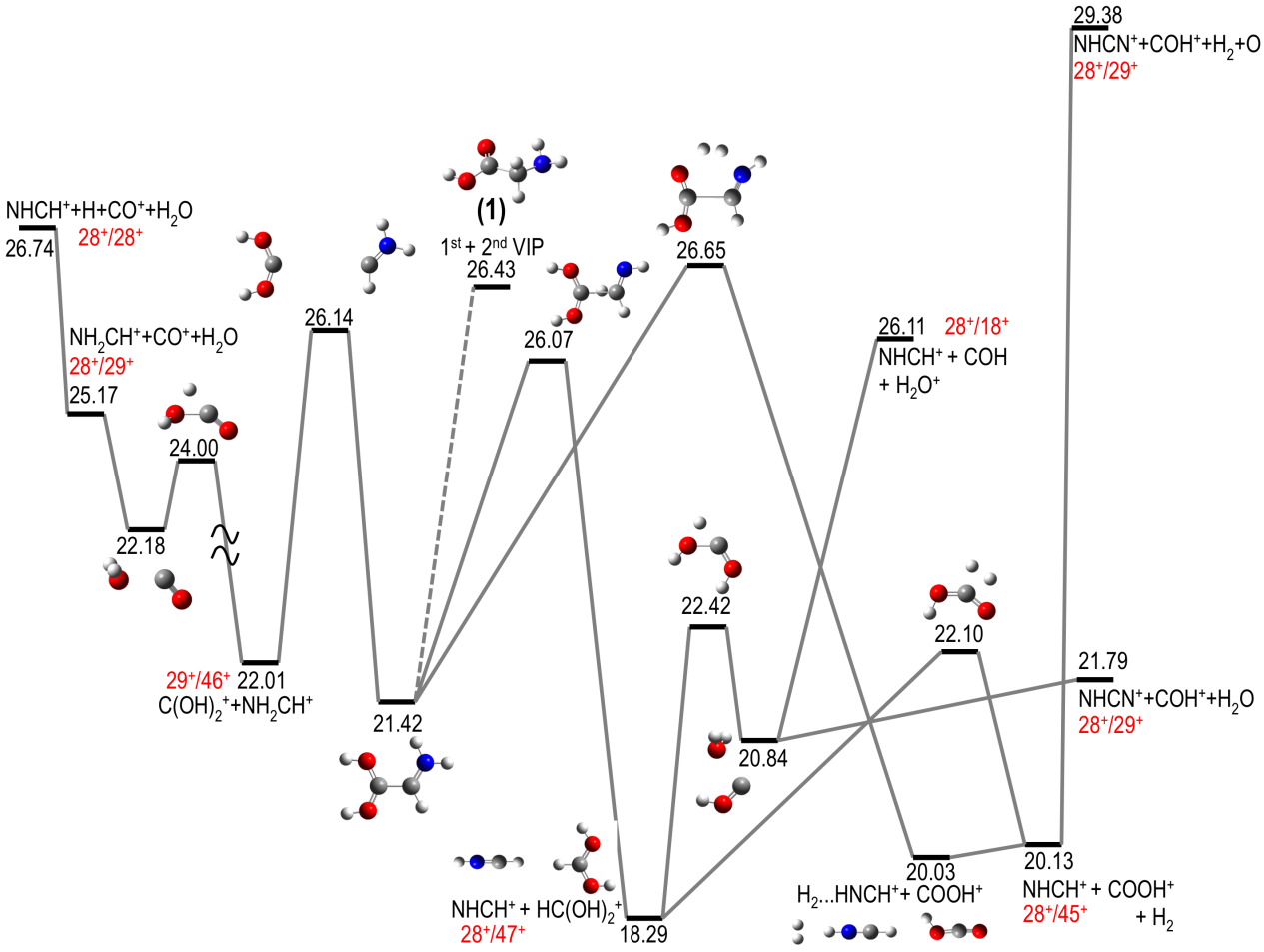

Figure 4: Fragmentation pathways for doubly positively charged glycine. Channels leading to coincident measurements after Coulomb explosion from the geminal diol isomer are shown. Relative energies, ΔE, are given in eV at the DFT-B3LYP/6-311++G(d,p) level of theory including the zero point energy correction with respect to the most stable isomer of the neutral molecule. Key structures as cited in the article are labelled as (1), (2), etc. Coincidence notation is also included, e.g. $30^+/45^+$. In this figure, the fragmentation pathways after ultrafast H migration leading to to coincident measurements are given.

Energy (eV)	% Percentage of each process							
	Coulomb Explosion		Isomerization		Others			
	(a)	(b)	(c)	(d)	(e)	(f)	(g)	(h)
0.027	100%	0%	0%	0%	0%	0%	0%	0%
0.136	100%	0%	0%	0%	0%	0%	0%	0%
0.272	100%	0%	0%	0%	0%	0%	0%	0%
0.544	100%	0%	0%	0%	0%	0%	0%	0%
0.816	100%	0%	0%	0%	0%	0%	0%	0%
1.089	100%	0%	0%	0%	0%	0%	0%	0%
1.361	100%	0%	0%	0%	0%	0%	0%	0%
1.633	99%	0%	0%	1%	0%	0%	0%	0%
1.905	98%	0%	0%	2%	0%	0%	0%	0%
2.177	98%	0%	0%	2%	0%	0%	0%	0%
2.449	98%	1%	1%	0%	0%	0%	0%	0%
2.722	98%	0%	1%	1%	0%	0%	0%	0%
2.994	94%	2%	1%	1%	1%	1%	0%	0%
3.266	92%	4%	0%	4%	0%	0%	0%	0%
3.538	91%	5%	0%	4%	0%	0%	0%	0%
3.810	91%	3%	0%	5%	0%	0%	1%	0%
4.082	86%	5%	1%	4%	1%	1%	1%	1%
Total – average	96.76%	1.18%	0.24%	1.41%	0.12%	0.12%	0.12%	0.06%
	97.94%		1.65%		0.42%			

Table 2: Statistics for each value of the excitation energy, summed over all the considered isomers, percentage of the observed exit channels in the molecular dynamics symulations: (a) $NH_2CH_2^+ + COOH^+$, (b) $NH_3CH^+ + COOH^+$, (c) $[NH_2 - CH - C(OH)_2]^{2+}$, (d) $[NH_3 - CH - COOH]^{2+}$, (e) $NH_2CHCOOH + +H^+$, (f) $NH_3CHOH^{2+} + CO$, (g) $NH_2CHCO^+ + H_2O^+$ / $NH_2CHCO^{2+} + H_2O$, (h) $NH_2C^+ + H_2 + COOH^+$.

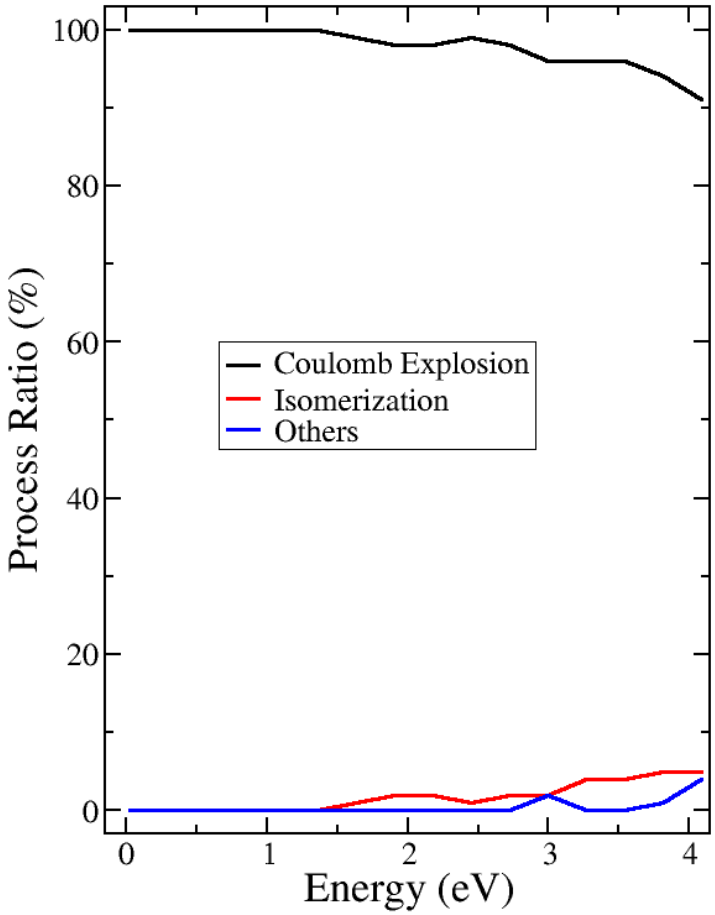

Figure 5: Percentage of processes as a function of the internal excitation energy: Coulomb explosion processes (a) and (b), Isomerization processes (c) and (d), and Other processes (e-h).